Published in final edited form as:
Biochim Biophys Acta. 2014 January ; 1840(1): 507–515. doi:10.1016/j.bbagen.2013.10.011.

Photodamage of Lipid Bilayers by Irradiation of a Fluorescently Labeled Cell-Penetrating Peptide

Igor Meerovich, **Nandhini Muthukrishnan**, **Gregory A. Johnson**, **Alfredo Erazo-Oliveras**, and **Jean-Philippe Pellois**
Department of Biochemistry and Biophysics, Texas A&M University, College Station, TX 77843

Abstract

Background—Fluorescently labeled cell-penetrating peptides can translocate into cells by endocytosis and upon light irradiation, lyse the endocytic vesicles. This photo-inducible endosomolytic activity of Fl-CPPs can be used to efficiently deliver macromolecules such as proteins and nucleic acids and other small organic molecules into the cytosol of live cells. The requirement of a light trigger to induce photolysis provides a more spatial and temporal control to the intracellular delivery process.

Methods—In this report, we examine the molecular level mechanisms by which cell-penetrating peptides such as TAT when labeled with small organic fluorophore molecules acquire a photo-induced lytic activity using a simplified model of lipid vesicles.

Results—The peptide TAT labeled with 5(6)-carboxy-tetramethylrhodamine binds to negatively charged phospholipids, thereby bringing the fluorophore in close proximity to the membrane of liposomes. Upon light irradiation, the excited fluorophore produces reactive oxygen species at the lipid bilayer and oxidation of the membrane is achieved. In addition, the fluorescent peptide causes aggregation of photo-oxidized lipids, an activity that requires the presence of arginine residues in the peptide sequence.

Conclusions—These results suggest that the cell penetrating peptide plays a dual role. On one hand, TAT targets a conjugated fluorophore to membranes. On the other hand, TAT participates directly in the destabilization of photosensitized membranes. Peptide and fluorophore therefore appear to act in synergy to destroy membranes efficiently.

General Significance—Understanding the mechanism behind Fl-CPP mediated membrane photodamage will help to design optimally photo-endosomolytic compounds.

Keywords

Cell-penetrating peptide; photochemical internalization; photolysis; liposomes

1. Introduction

Intracellular delivery of macromolecules such as proteins and nucleic acids is important for therapeutic applications and various cell biology applications. A strategy used for

Corresponding Author: Jean-Philippe Pellois, Biochemistry and Biophysics Bldg., Room 436A, 300 Olsen Blvd, Texas A&M University, College Station, TX, 77843-2128., Telephone: +1 979-845-0101, Fax: +1 979-862-4718, pellois@tamu.edu.

macromolecular delivery into live cells is Photochemical Internalization (PCI). PCI utilizes light-responsive and membrane disruptive chemical agents known as photosensitizers [1, 2]. Typically, cells are first incubated with a photosensitizer and a cell-impermeable macromolecule of interest. During incubation, both the photosensitizer and macromolecule accumulate inside endosomes upon endocytic uptake by the cells. Following incubation, cells are irradiated with visible light and the photosensitizer causes disruption of the membrane of endosomes by generating reactive oxygen species (ROS) locally. The macromolecule present in the lumen of these organelles can subsequently escape into the cytosol of cells and exert a biological function [1]. One of the attractive aspects of this approach is that endosomal escape is induced only in the presence of a light-trigger. As a result, the delivery process can be temporally and spatially modulated and controlled [3]. More importantly, endosomal release, which is usually a limiting step in delivery strategies that utilize endocytosis as a route of cellular entry, is relatively efficient with the PCI technique.

Photosensitizers used for PCI have typically included phthalocyanine or porphyrin derivatives that localize within endocytic organelles [4]. When irradiated, these photosensitizers generate reactive oxygen species (ROS) which can then damage and lyse the membrane of endosomes [5]. Interestingly, fluorescently labeled cell-penetrating peptides (Fl-CPPs) have been shown to also possess a photo-endosomolytic activity. Upon endocytosis and irradiation, the cell-penetrating peptides (CPPs) TAT or R9 labeled with fluorescein, tetramethylrhodamine (TMR), Alexa fluors and Cy3 lyse endosomes and subsequently deliver proteins and nucleic acids to the cytosol of live cells successfully [3, 6–8]. The porphyrin photosensitizer- CPP conjugates have been applied previously for PCI and other photodynamic therapy related applications [9–12]. While photosensitizers and Fl-CPPs share a similar photo-endosomolytic activity, the mechanisms involved in membrane disruption appear to be quite different. Like PCI photosensitizers, the fluorophores used to label CPPs can generate ROS upon irradiation. In particular, singlet oxygen can be formed upon irradiation by transfer of energy from the fluorophore in triplet excited state to dissolved molecular oxygen [13]. However, while photosensitizers generally generate singlet oxygen in relatively high yields, the fluorophores used to label CPPs typically have very poor singlet oxygen quantum yields [14, 15]. Studies with membrane models such as the plasma membrane of red blood cells (RBCs) indicate that generation of ROS is indeed involved in the photolytic activity of Fl-CPPs [7, 16]. Yet, these studies also suggest that the CPP moiety acts in synergy with the singlet oxygen-generating fluorophores to disrupt membranes efficiently [16]. For instance, RBCs irradiated in the presence of TMR-TAT undergo a dramatic shrinkage while RBCs irradiated with conventional photosensitizers such as hematoporphyrin do not. Moreover, the photolysis of RBCs mediated by a photosensitizer is greatly enhanced if unlabeled TAT or R9 are added during or after irradiation. Because these effects are not observed in the dark, these results suggest that CPPs destabilize biological membranes after photo-oxidation of membranous components takes place. The molecular details of this phenomenon remain however unclear. Moreover, the membrane components involved in the photolysis induced by Fl-CPPs have not been identified.

In this report, we use large unilamellar vesicles (LUVs) as simplified membrane models to evaluate the implication of lipids in TMR-TAT mediated photolysis. In particular, we test the hypothesis that TMR-TAT promotes lipid oxidation by local generation of ROS. We also test whether membrane destabilization by the peptide contributes to photolysis. We demonstrate that TMR-TAT destroys liposomes upon light irradiation. First, TAT brings TMR in close proximity to lipid bilayers by binding to negatively charged lipids. Excitation of TMR then causes singlet oxygen and superoxide formation followed by lipid oxidation. Importantly, lipid oxidation is not sufficient to account for liposomes destruction. Instead,

the arginine-rich CPP promotes the aggregation of photo-oxidized LUVs and accelerates their lysis. Our results therefore reveal a unique synergy between oxidized lipids and CPPs that leads to enhanced photolysis.

2. Material and methods

2.1. Materials used

All peptide synthesis reagents were obtained from Novabiochem (EMD/Merck, Darmstadt, Germany). The fluorophores 5(6)-carboxytetramethylrhodamine and 5(6)-carboxyeosin Y were purchased from Novabiochem and Marker Gene Technologies (Eugene, OR) respectively. Eosin Y, tetramethylrhodamine, Rose Bengal, *p*-nitrosodimethylaniline (RNO), sodium azide, α-tocopheryl acetate, imidazole, salts for buffer preparation were received from Sigma-Aldrich (St. Louis, MO). For liposome preparation, 1-stearoyl-2-oleoyl-sn-glycero-3-phospho-choline (PC), 1,2-dioleoyl-sn-glycero-3-phosphocholine (PC'), 1,2-dioleoyl-sn-glycero-3-phospho-L-serine (PS), bis-(mono-oleoylglycero)-phosphate (BMP) and cholesterol were bought from Avanti Polar Lipids (Alabaster, AL).

Peptide synthesis—The peptides TAT (GRKKRRQRRRG-NH_2), R9 (GRRRRRRRRR-NH_2) and K9 (KKKKKKKKK-NH_2) were prepared using Fmoc solid-phase chemistry on a 0.72 mmol scale using rink amide MBHA resin to obtain C- terminal amides.. The amino acids Fmoc-Gly-OH, Fmoc-Arg(Pbf)-OH, Fmoc-Lys(Boc)-OH, Fmoc-Gln-OH, 5(6)-carboxy-tetramethylrhodamine and 5(6)-carboxyeosin Y were used to synthesize the required peptides. All reactions were performed at room temperature and with constant agitation using dry N2 gas. The Fmoc on the peptide resin was first deprotected by addition of a 20% piperidine solution in DMF. The deprotection was performed twice for 5 min and 15 min respectively followed by DMF washes each time. Then, the amino acids were added on the resin using a coupling reaction. The coupling reactions were carried out using a mixture of the Fmoc amino acid (2.88 mmol), HBTU (1.06 g, 2.80 mmol) and DIEA (1.25 mL, 7.2 mmol) in DMF for 3 hr. The resin was washed with DMF after each coupling step and the Fmoc-deprotected before each coupling reaction. After synthesis of the peptide on the resin corresponding to TAT, R9 or K9 sequence, 20% piperidine in DMF was added for 1×5 and 1×15 min to deprotect the Fmoc on the N terminal residue of the peptide while keeping the side-chain protecting groups on the amino acids intact. The fluorophores were then coupled onto the peptide by reacting the peptide with a mixture of 5(6)-carboxy-tetramethylrhodamine or 5(6)-carboxyeosin Y (2.88 mmol), HBTU (1.06 g, 2.80 mmol) and DIEA (1.25 mL, 7.2 mmol) in DMF overnight.

After assembly of the Fl-CPP on the solid support, the resin was treated with a solution of TFA containing 2.5% H_2O and 1% triisopropylsilane for 2 hr in order to deprotect all the side chains on the peptide and cleave the Fl-CPP off the resin. The crude Fl-CPPs present in the TFA solution were then washed with cold anhydrous Et2O to achieve peptide precipitates. The crude peptides were then dissolved in aqueous acetonitrile and lyophilized. Fl-CPPs were purified using semi-preparative HPLC and their purity was confirmed by mass spectrometry (MALDI-TOF) analysis. TAT expected mass: 1451.92 Da, observed mass: 1452.41 Da; R9 expected mass: 1478.96 Da, observed mass: 1479.52 Da; K9 expected mass: 1169.88 Da, observed mass: 1170.96 Da; TMR-TAT expected mass: 1865.07 Da, observed mass: 1866.1 Da; TMR-K9 expected mass: 1583.0 Da, observed mass: 1583.30 Da; TMR-R9 expected mass: 1893.20 Da, observed mass: 1894.4 Da, The pure lyophilized peptides were dissolved in water to make 1 mM stock solutions that were diluted to desired working concentrations in PBS (NaCl 137 mM, KCl 2.7 mM, Na_2HPO_4 10 mM, KH_2PO_4 1.8 mM; adjusted to pH 7.4) for experiments.

Preparation of liposomes—Lipids in chloroform were mixed in a glass vial at molar ratios of 7:3 PC:cholesterol for neutral liposomes and 4:3:3 PC:PS:cholesterol or 4:3:3 PC:BMP:cholesterol for negatively charged liposomes. Alternatively, neutral liposomes were prepared with a composition of 4:3:3 PC:PC':cholesterol, in order to generate neutral LUVs that contain the same amount of unsaturated lipids as their negatively charged counterparts. Lipid films were prepared by evaporating the solvent from the mixture using a flow of nitrogen gas, then removing trace solvent by freeze-drying. The films were hydrated with only PBS buffer or buffer solution of calcein (60 mM) by vigorous vortexing and then allowed to swell for 2 hours at 10°C under nitrogen to obtain multilamellar lipid vesicles. Liposomes were extruded through Nuclepore polycarbonate membranes (Whatman, Clifton, NJ) with pore sizes of 100 nm (21 passes; for fluorometric studies) or 200 nm (11 passes; for turbidometry studies) using a Mini-Extruder device (Avanti Polar Lipids, Alabaster, AL). The respective size distribution of liposomes was on average 140 and 236 nm, as determined by dynamic light scattering using a Zeta Sizer device (Malvern instruments, Worcestershire, UK). The extruded large unilamellar vesicles (LUVs) were stored at 4°C and used within two weeks of preparation.

When required for calcein-leakage experiments, calcein-loaded LUVs were separated from non-entrapped fluorophore by gel filtration on Sephadex G-50 (GE Healthcare, Pittsburgh, PA) column (2.5×14 cm). Additionally, for experiments performed with cis-parinaric acid (PnA), the latter was added in ethanol solution to the lipid mixtures listed above at 1% mol. to the total lipids. PnA-containing lipid mixtures were dried with a flow of nitrogen and freeze-dried. Lipids were then re-dissolved in a minimum amount of chloroform and dried again, in order to provide a homogeneous distribution of constituents. PnA-containing LUVs were hydrated as described above and extruded through 100 nm pore size Nuclepore membranes (21 passes). Because of their sensitivity to oxidative damage, the PnA-containing LUVs were used within 40 hours of preparation.

Fl-CPP binding to liposomes and fluorescence anisotropy—The binding of peptides to lipid bilayers can be described by an apparent molar partition coefficient K [17, 18]. Our measurements used molar concentrations of lipid [L] much greater than that of the peptide bound to the liposomes $[P]_b$. Under these conditions:

$$[P]_b = K[P][L] \quad (1)$$

Because the peptides might permeate membranes, [L] is the total molar concentration of lipid in the solution. In addition, the free peptide molar concentration [P] can be substituted for $[P]_{tot}$-$[P]_b$ in Eq.1 to obtain:

$$[P]_b/[P]_{tot} = K[L]/(1+K[L]) \quad (2)$$

where $[P]_{tot}$ is the total molar concentration of peptide in solution. To obtain K, the binding of Fl-CPPs to lipid bilayers was determined by titrating the samples with neutral or anionic LUVs and determining the change of the fluorescence anisotropy for different total lipid concentrations. Fluorescence anisotropy was determined using a SLM-8000C fluorometer (SLM Instruments, Bath, UK) upgraded with the Phoenix package (ISS, Champaign, IL) and Vinci v.1.6 PC software (ISS). The contributions of light scattering and inner filter effect were minimized by filtering out the excitation wavelength from the emission beam and by using a low concentration of Fl-CPPs (0.25 to 2 μM). Titration with liposomes and acquisition of fluorescence anisotropy were performed in 3 mm optical path micro-cuvettes with 100 nm liposomes. Fluorescence anisotropy (*r)* was calculated automatically by Vinci v.1.6 PC software from four intensities of fluorescence measured under different positions

of excitation and emission polarizers according to reported protocols [19]. Titration of each Fl-CPP was repeated at least three times and average r values were determined for each data point. Since binding of conjugates to liposomes caused change of their fluorescence quantum yield due to change of environment, fraction bound was calculated from anisotropy-concentration dependencies using the following equation:

$$f_B = \frac{r - r_F}{(r - r_F) + R \cdot (r_B - r)} \quad (3)$$

where f_B is the bound fraction of fluorophore; r, r_F and r_B – respectively values of fluorescence anisotropy at some current point, for fully free and fully bound fluorophore (on start and saturation of titration), and R is ratio of intensities of fluorescence of fully bound and fully free fluorophore forms, evaluated after correcting for dilution measured total fluorescence intensity values (determined by Vinci software in process of anisotropy calculation; derived from emission intensities for parallel and perpendicular polarizers orientations I_{VV} and I_{VH} as $I_{VV} + 2 \cdot G \cdot I_{VH}$, where G is the device-specific parameter) [20]. The resulting binding curves were plotted and fitted to a one site-specific binding model using the GraphPad Prism v.5 software. The reciprocal of K, the dissociation constant K_d, was derived from these plots and used to compare the relative binding efficiency of the conjugates to lipids. K_d corresponds to the total molar concentration of lipid in solution that causes binding of half of the Fl-CPP present.

Photodamage of liposomes—Samples were irradiated for a given amount of time using a 600 W Utilitech halogen lamp, filtered via 1.5-inch water filter, diffusing glass and green optical cast plastic filter NT46-624 (Edmund Optics, Barrington, NJ) with a maximum transmission in the range of 450 to 580 nm. The final photon flux output is 3.3×10^{17} photons$\times s^{-1} \times cm^{-2}$. This photon flux is approximately 3200 fold less than what has been reported for the irradiation of Fl-CPP trapped inside endosomes of live cells on an epifluorescence microscope (irradiance is high because of the focusing of light beam after 100× objective). For comparison purposes, 40 min irradiation with the described set-up is equivalent to 0.75 sec irradiation on a microscope, a time scale at which most endosomes are photolysed [7].

Disruption and permeabilization of lipid bilayers upon photolytic treatment were evaluated using a calcein leakage assay (see details in Supporting Information, SI). The destruction of LUVs mediated by the Fl-CPPs (2 μM) was evaluated by turbidometry [21, 22]. LUVs were diluted to the final concentration of 800 μM of total lipids in PBS. These liposome solutions are turbid and consequently have an optical density at 750 nm. Fluorophores or Fl-CPPs were added to these samples at different final concentrations and the samples were optionally supplied the lipophilic antioxidant *α*-tocopherol (60 μM). After irradiation, samples were subjected to low speed centrifugation to remove aggregates from soluble LUVs. Photodestruction was monitored by measuring the optical density of the solutions at 750 nm using UV-1700 PharmaSpec (Shimadzu, Kyoto, Japan) spectrophotometer with 1 cm quartz cuvettes.

Evaluation of production of singlet oxygen—A spectrometric RNO assay was performed to evaluate the formation of singlet oxygen upon light irradiation of TMR-TAT, Eosin Y and Rose Bengal (RB) in aqueous solution [23]. Solutions of RNO (50 μM) and imidazole (10 μM) were prepared in PBS and mixed with Fl-CPPs or RB, a photosensitizer with a reported quantum yield of singlet oxygen of 0.76 in water, was used as a positive control [23]. The concentration used in this assay were 7 μM for TMR-TAT, Eosin Y, and RB [24]. The decrease in the absorbance of RNO was monitored using a plate reader (450

nm) at periodic intervals. The conditions of irradiation for this experiment were the same as described for the turbidometry assay.

Evaluation of production of superoxide—The formation of superoxide was monitored by the nitro blue tetrazolium (NBT) method [25–28]. Reduction of NBT by superoxide (O_2^-) results in formation of an insoluble formazan, which can be detected by absorbance at 560–600 nm. Each sample was prepared in phosphate buffer containing NBT (80 μM), NADH (10 mM), and EDTA (1 mM). Samples were also supplemented with the desired concentration of photosensitizing agent, and without or with 10 mM of the quenchers tiron (4,5-Dihydroxy-1,3-benzenedisulfonic acid disodium salt) or mannitol. Samples were irradiated as described for the turbidometry assay. After irradiation, each sample was diluted in DMSO 5-fold. The absorbance of the resulting solution was measured at 600 nm (at this wavelength, the contribution of TMR and eosin Y is negligible). The absorbance reported represents the absorbance of each sample after subtraction of the absorbance measured before irradiation.

Detection of photo-oxidation in the lipid bilayer—Formation of oxidative conditions during photolysis with various Fl-CPPs under different conditions was studied using liposomes with lipid composition additionally supplied with 1 %mol. of 9Z,11E,13E,15Z-octadecatetraenoic acid (cis-Parinaric acid, PnA). Experiments were performed with freshly prepared liposomes at final concentration of 800 μM by total lipids, with and without addition of Fl-CPPs to the final desired peptide to total lipid ratio (e.g. 2 μM for P:L of 1:400), irradiated with the Oriel model 67705 Hg-Xe arc light source (Oriel Instruments, Stratford, CT) equipped with HQ 560/55 filter (Chroma Technology Corp., Bellows Falls, VT) providing an irradiance with the final photon flux output of 1.9×10^{17} photons$\times s^{-1}\times cm^{-2}$. Oxidation of PnA was evaluated by measuring the decrease of its fluorescence emission at 410 nm (Ex = 320 nm), from spectra collected using a SLM-8000C fluorometer (SLM Instruments) operated with Vinci v.1.6 PC software (ISS). To account for the fact that LUVs might aggregate upon irradiation (as shown in Figure 1) and that this might cause a reduction in PnA signal, the fluorescence of PnA was recorded before or after of 0.2% of the detergent Triton X. The results obtained before or after addition of detergents were similar in all cases, indicating that the loss of fluorescence of PnA presented in Figures 3,4 and 5 is not due to an overall loss of the amount of LUVs present in solution. The data represented in the Figures are those obtained prior to addition of Triton X. Oxidation of phospholipids during photolysis was additionally confirmed by reaction with redox-indicator N,N,N′,N′-tetramethyl-1,4-phenylene-diamine (see SI).

3. Results

TMR-TAT binds to negatively charged LUVs but not to neutral LUVs

While trafficking within the endocytic pathway of cells, one can expect that Fl-CPPs might encounter zwitterionic (e.g. PC) as well as anionic phospholipids (e.g. PS). To begin our studies, we therefore characterized the binding of TMR-TAT to LUVs composed of PC and PC/PS (all LUVs also contain 30 %mol. of cholesterol as this reflects the lipid composition of mammalian membranes [29, 30]). The association of TMR-TAT with lipid bilayers was investigated by steady-state fluorescence anisotropy. The anisotropy of TMR-TAT increased significantly upon addition of negatively charged PS-containing LUVs but remained unchanged upon addition of PC liposomes. The data obtained were fitted to a one site-specific binding model and the dissociation constant of TMR-TAT for PC/PS liposomes was determined to be 164.6±14.7 μM (Figure 1A). In addition, the fluorescence anisotropy of TMR alone (with or without 5(6)-carboxy moieties) was unaffected by addition of

liposomes. This in turn suggests that TMR does not bind to LUVs and that the binding of TMR-TAT to negatively charged liposomes is primarily mediated by the CPP.

TMR-TAT destroys negatively charged LUVs in a light-dependent manner

In order to establish whether irradiation of TMR-TAT leads to the disruption of lipid bilayers, a leakage assay that monitors the release of calcein from the lumen of liposomes was initially performed (Figure S1). An increase in calcein fluorescence was detected when PC/PS LUVs were irradiated in the presence of TMR-TAT. On the other hand, this was not observed with PC LUVs, when TMR-TAT is absent, or when the sample is kept in the dark. These data therefore suggest that TMR-TAT mediates calcein escape from negatively charged LUVs upon irradiation. However, irradiation was also accompanied by the apparent precipitation of components from the solution, thereby preventing the quantitative analysis of these results. To test whether TMR-TAT might be involved in this phenomenon, free liposomes (i.e. not loaded with calcein) were incubated with TMR-TAT and irradiated. After short-spin centrifugation to remove potential precipitates, the optical density of the liposomal suspension was monitored at 750 nm as a function of irradiation time. Our rationale was that this turbidometry assay could be used to monitor whether liposomes aggregated during irradiation as precipitation would be accompanied by a loss of light scattering [21, 22].

As shown in Figure 1B, irradiation of PC/PS LUVs in the presence of TMR-TAT caused a significant reduction in turbidity of the sample. In contrast, the turbidity of a suspension of PC LUVs was not significantly affected under similar conditions. In addition, irradiation of PC/PS LUVs irradiated with TMR alone, TAT alone or TAT mixed with TMR (1:1 stoichiometry) did not lead to a loss of turbidity (Figure 1B). Finally, the turbidity of all samples remained unchanged after incubation in the dark (Figure S2). Together, these data therefore suggest that loss of turbidity requires conjugation of TMR to TAT, binding of TMR-TAT to liposomes, and light excitation of TMR-TAT.

To further investigate the origin of the loss of turbidity observed, liposomal suspensions were examined by bright field and fluorescence microscopy. As shown in Figure 1C, aggregates could be observed in irradiated solutions containing TMR-TAT and PC/PS LUVs. These aggregates were brightly fluorescent, indicating that the labeled-peptide is one of the components present (Figures 1C and S2). At high doses of light, the formation of large colored aggregates was visible to the eye (Figure 1D). To confirm that the loss of turbidity observed is due to a loss of lipid content, the relative change of lipid concentration of LUV suspensions irradiated in the presence of TMR-TAT was evaluated. As with the turbidity assay, samples were short-spinned at low speed after irradiation to remove possible aggregates formed and the supernatants were analyzed for phospholipid content with an ammonium ferrothiocyanate assay. As shown in Figure S3, the phospholipid content of the supernatants decreases with irradiation time at a rate proportional to the loss of turbidity previously observed. Overall, these data therefore indicate that TMR-TAT and liposomes form large aggregates after light irradiation and that the loss of turbidity measured is a result of this aggregation process.

Photodestruction of liposomes is mediated by the formation of reactive oxygen species in close proximity to lipid bilayers and by oxidation of lipids

To gain some mechanistic insights on how TMR-TAT mediates the liposome photo-destruction observed, the dependence of this activity on oxygen was first assessed. A turbidometry assay was performed on suspensions of PC/PS LUVs irradiated with TMR-TAT in buffer saturated with argon or oxygen. As shown if Figure 2A, irradiation of samples saturated with argon did not cause a loss of turbidity. In contrast, samples saturated

in oxygen led to a decrease in turbidity similar to that observed in Figure 1 where air-equilibrated buffer is used. The requirement for both light and oxygen suggested that TMR-TAT photosensitize LUVs with the formation of singlet oxygen (Type II) or superoxide (Type I mechanism) as primarily generated ROS, with molecular oxygen being respectively an acceptor of either electron or energy transfer from the excited fluorophore/photosensitizer molecule [31].

In order to detect whether TMR-TAT might produce singlet oxygen upon irradiation, a RNO assay was performed [23]. The photosensitizer Rose Bengal (RB) was used as a positive control. In addition, 5(6)-carboxyeosin Y, another halogenated xanthene derivative known to produce singlet oxygen upon irradiation, was conjugated to TAT to improve the solubility of the photosensitizer in water. Eosin-TAT was then used as an additional control. Upon irradiation, production of singlet oxygen from TMR-TAT could be detected (Figure 2B). Consistent with the small triplet state quantum yields of TMR reported in the literature, singlet oxygen production was however very inefficient in comparison to Eosin-TAT (singlet oxygen quantum yield of 0.57 for Eosin Y) or RB (singlet oxygen quantum yield 0.72–0.79 [32–34]). In order to determine whether TMR-TAT also produces superoxide upon irradiation, a NBT assay was utilized. Eosin Y has been previously shown to produce superoxide in addition to singlet oxygen upon excitation [35]. Eosin-TAT was therefore used a positive control in this assay as well (singlet oxygen does not interfere with the NBT assay [25]). As shown in Figure 2C, irradiation of TMR-TAT caused a chemical reduction of NBT, as observed by an increase in absorbance,. NBT reduction was inhibited by addition of the superoxide quencher tiron, suggesting that superoxide is indeed detected in this assay (Figure 2D). However, a concern is that the hydroxyl radical, a ROS that can potentially be produced from superoxide, might interfere with the NBT assay (tiron can also potentially quench the hydroxyl radical[36]). To address this issue, mannitol, a quencher with specificity for the hydroxyl radical over other ROS, was added to the NBT assay [37, 38]. As shown in Figure 2D, addition of mannitol had a relatively small effect on the chemical reduction of NBT mediated by TMR-irradiation. These results therefore indicate that the NBT reduction observed is mainly reporting formation of superoxide. Together, these data suggest that TMR-TAT produces both singlet oxygen and superoxide upon light irradiation.

Next, we interrogated whether TMR-TAT might photosensitize LUVs by causing oxidative damage in the lipid bilayer. Singlet oxygen and superoxide are known to oxidize unsaturated lipids to form lipid hydroperoxides [39]. In order to detect whether irradiation of TMR-TAT resulted in the formation of lipid hydroperoxides, a colorimetric assay was performed with the peroxide indicator TMPD. TMPD is oxidized by lipid hydroperoxides and this can be detected by so called “Wurster’s blue” coloration and an increase in the absorbance of the compound at 610 nm [40–42]. For these experiments, LUVs were incubated and irradiated with TMR-TAT, TMPD was added to the sample after 40 min of irradiation, and the absorbance of TMPD was measured. As shown in Figure 3A, PC LUVs irradiated with TMR-TAT in PBS did not give rise to a TMPD signal markedly higher than PBS alone. In contrast, PC/PS LUVs subjected to a similar treatment led to a five-fold increase in TMPD absorbance at 610 nm. This was not observed when the sample was kept in the dark. Together, these results are consistent with the notion that TMR-TAT oxidizes lipids upon irradiation and that binding to the lipid bilayer is required for this effect.

While the TMPD assay confirmed the presence of lipid peroxides, this assay is not very sensitive and oxidized TMD was detected only after irradiation times of 30–40 min. At this light dose, the turbidity of negatively charged LUVs is significantly reduced. This therefore raised the concern that lipid hydroperoxides formation might be a consequence of TMR-TAT/lipid aggregation as opposed to a cause. To address this issue, the effect of α-tocopherol, a lipophilic antioxidant, on LUV photo-destruction was determined. When

added to PC/PS LUVs, α-tocopherol inhibited the loss of turbidity mediated by TMR-TAT irradiation (Figure 3B).

In a complementary assay, the lipid peroxidation reporter cis-parinaric acid (PnA) was incorporated into LUVs (1%). PnA is a conjugated polyunsaturated fatty acid that emits a fluorescence signal at 410 nm upon excitation at 320 nm. PnA is sensitive to oxidative damage and oxidation results in loss of fluorescence. PnA-LUVs and TMR-TAT samples were irradiated and the fluorescence of PnA was monitored over time. Experiments were performed with P:L ratio of 1:400. The total duration of irradiation was limited to 4 min of light exposure, so as to assess the activity of TMR-TAT under conditions where the loss of turbidity was minimal (the light of irradiation set-up used here is also less intense than that used for the turbidometry assay, see material and methods for details). As shown in Figure 3B, irradiation of PnA-liposomes with TMR-TAT caused a rapid loss of PnA fluorescence when incubated with PC/PS LUVs. PC LUVs were not significantly oxidized by irradiation with TMR-TAT, suggesting that TMR-TAT present in solution and not bound to lipids does not contribute to oxidative damage in the lipid bilayer. These data also establish that oxidation can be detected before lipid aggregation is observed and that inhibiting oxidation inhibits LUV photodestruction.

Photodestruction of liposomes with TMR-TAT is mediated by the action of the cell-penetrating peptide

Our previous data suggested that photo-oxidation of the lipid bilayer is required for LUV photo-destruction. Next, we tested whether photo-oxidation is sufficient for this phenomenon. RB possesses a spectral maximum of excitation similar to that of TMR-TAT (see Figure S4) and also produces singlet oxygen and superoxide. In addition, RB is lipophilic and readily associates with lipid bilayers (see Table S1, K_d determined with PC/PS LUVs is 213.8 ± 26.6 μM). We therefore reasoned that, if lipid bilayer photo-oxidation is sufficient for the formation of lipid aggregates, irradiation of RB should lead to a loss of turbidity similar to that seen with TMR-TAT. To test this idea, the activity of RB was first quantified with the PnA assay previously described. As shown in Figure 4A, irradiation of RB (2 μM) incubated with PC/PS LUVs containing 1% PnA (P:L=1:400) also led to a rapid loss of PnA fluorescence, with higher rate than that of TMR-TAT, consistent with the notion that RB is a photosensitizer more effective at generating singlet oxygen than TMR. Yet, irradiation of LUVs incubated with RB did not lead to significant loss of turbidity (Figure 4B). Overall, these data therefore suggest that, despite being more photo-oxidative than TMR-TAT, RB is unable to cause lipid aggregation.

These results therefore raised the possibility that the peptide moiety of TMR-TAT, in addition to bringing TMR in close proximity to the lipid bilayer, might contribute to lipid aggregation. To test this hypothesis, the peptides TMR-K9 and TMR-R9 were synthesized. Like TMR-TAT, TMR-K9 and TMR-R9 are positively charged (both possess overall charge of +9) and both species bind to PC/PS LUVs but not to PC LUVs (Table S1, K_d of binding with PC/PS LUVs were 153.0 ± 10.1, and 202.8 ± 19.3 mM for TMR-R9 and TMR-K9, respectively). In order to compare the activity of the peptides quantitatively, TMR-TAT, TMR-R9 and TMR-K9 were incubated with PC/PS LUVs at a P:L ratio of 1:1400 providing conditions where all three species are 92–93% bound to lipids. Under these conditions, irradiation of TMR-R9 led to a loss of turbidity similar to that observed with TMR-TAT. In contrast, TMR-K9 was unable to reproduce this effect. In addition, a PnA assay performed under similar conditions showed that TMR-K9, while slightly less active than TMR-R9 and TMR-TAT, could nonetheless promote the rapid oxidation of the PnA probe. The activities of TMR-R9 and TMR-K9 were also compared at a P:L ratio of 1:400. Under these conditions, the fraction of TMR-R9 bound to liposomes is greater than that of TMR-K9. However, in both cases, the density of peptide on the surface of liposomes should be

increased and the contribution of the peptide to membrane destabilization should be increased as well. Consistent with this idea, the loss of turbidity mediated by TMR-R9 was significantly faster at a 1:400 than at a 1:1400 P:L ratio. However, TMR-K9 remained inactive under these more stringent conditions. Together, these results therefore indicate that, like RB, TMR-K9 does not cause lipid aggregation after oxidation of the lipid bilayer. Instead, because TAT and R9 are both arginine-rich peptides, these data suggest that arginine residues are important for this photo-destructive activity.

Because the binding of TMR-R9 to PC/PS LUVs is presumably mediated by interactions between arginine side chains and the negatively charged polar head of PS, we next tested whether the photo-induced CPP/lipid aggregation observed was specific to LUVs containing PS. Because a fluorescent CPP might encounter the phospholipid bis(monoacyl-glycero)-phosphate (BMP) inside late endosomes, the photo-induced activity of TMR-R9 towards PC/BMP LUVs was measured. Like PS, BMP is negatively charged but the structures and properties of these two lipids are otherwise quite different (e.g. propensity to induce membrane curvature). The binding affinity of TMR-R9 towards PC/BMP LUVs was determined by fluorescence anisotropy and was found to closely match that obtained with PC/PS LUVs (Figure S5, Table S1). In addition, irradiation caused a reduction of PnA fluorescence identical to that measured with PC/PS LUVs (supplemental info). Interestingly, loss of turbidity, while reduced in comparison to that obtained with PC/PS LUVs, was also observed when TMR-R9 was irradiated with PC/BMP LUVs. These data therefore suggest that the photodestructive capacity of Fl-CPPs such as TMR-R9 can affect LUVs composed of different negatively charged phospholipids.

Discussion

Our data establish that lipids are potential targets for the photolytic activity that Fl-CPPs exert on biological membranes. The CPPs TAT and R9, labeled with TMR could in particular cause liposomal leakage and destruction upon irradiation. Our results suggest that TMR produces singlet oxygen and superoxide upon irradiation and that the CPPs in the photolytic activity of Fl-CPPs by binding to negatively charged phospholipids. By bringing a fluorophore in close proximity to the lipid bilayer, ROS produced locally oxidizes lipids. In contrast, the fraction of Fl-CPP in solution, while still producing ROS upon irradiation, contributes little to lipid damage. For instance, no peroxidation and no PnA oxidation are detected when TMR-TAT does not bind to LUVs. These results are consistent with the notion that ROS such as singlet oxygen are both very reactive and short-lived and that, as a consequence, the oxidative damage they promote is more pronounced at the sites at which they are produced (i.e. where the fluorophore is in the case of a Fl-CPP) [39, 43].

While membrane binding and proximity to the bilayer are necessary for photodestruction, experiments with RB and TMR-K9 indicates that binding might not be sufficient to account for the photo-destruction of liposomes observed with TMR-TAT and TMR-R9. On one hand, TMR-K9, like TMR-R9, binds to negatively charged LUVs and photo-oxidizes PnA in the bilayer. On the other hand, irradiation of TMR-K9 did not lead to the destruction of PS-containing liposomes observed with TMR-R9 and TMR-TAT. These data therefore indicate that the photo-destruction of liposomes observed with labeled TAT and R9 might be mediated by the peptide themselves. In particular, the arginine-rich peptides might aggregate with oxidized lipids in a way that a lysine-rich analog cannot mimic. These results therefore support the notion that, while generation of ROS is necessary to initiate membrane photo-damage, it is the CPP moiety that contributes to the photo-destruction of LUVs observed. These results are therefore in good agreement with the photohemolysis study that has shown that RB can photolysis red blood cells without affecting membrane morphology while TMR-TAT causes photolysis as well as membrane shrinkage. It is now plausible that the

membrane shrinkage observed in this context is caused by the aggregation of TMR-TAT with oxidized lipids.

Overall, our results provide some mechanistic insights on how Fl-CPPs might lyse endosomes upon light irradiation. The fact that binding to negatively charged lipids is required for the lysis of liposomes suggests that Fl-CPPs might preferentially lyse endocytic organelles that contain negatively charged membranes. This could be the case for late endosomes as these organelles are uniquely enriched in BMP [44]. PS is typically thought to be present in the cytoplasmic leaflet of endocytic organelles but not in the luminal leaflet [45]. This is based on the idea that the PS asymmetry observed at the plasma membrane is maintained upon endocytosis. Whether an endocytosed Fl-CPP might encounter PS in the endocytic pathway remains therefore unclear. However, it has been shown that PS flip-flop is enhanced in liposomes containing oxidized PC [46]. It is therefore possible that, upon irradiation, Fl-CPPs initially cause minimal damage to the membrane of endosomes. If this initial damage however results in PS exposure on the luminal leaflet, the binding of a Fl-CPP to the membrane would dramatically increase. This, in turn, would further favor photo-induced membrane destruction. We propose that this model might serve as a starting point for the design of optimally photo-endosomolytic compounds. Finally, it should be noted that cells experience oxidative stress and that cellular membranes can contain oxidized lipids [39, 43]. Given the unique interactions detected in this report between CPPs and oxidized lipids, it is tempting to speculate that oxidized lipids might play an important role in the cell-penetration activity of CPPs (i.e. in the dark).

Supplementary Material

Refer to Web version on PubMed Central for supplementary material.

Acknowledgments

The authors thank Dr. M. Lasagna of the department of Biochemistry and Biophysics of Texas A&M University for his help and discussions regarding all fluorometric assays used in this work. This work was supported by Award Number R01GM087227 and R01GM087981 from the National Institute of General Medical Sciences, the Norman Ackerman Advanced Research Program, and the Robert A. Welch foundation (Grant A-1769).

Abbreviations

PCI	photochemical Internalization
BMP	bis(monoacylglycero)-phosphate
CPP	cell-penetrating peptide
Fl-CPP	fluorophore/cell-penetrating peptide conjugate
LUV	large unilamellar vesicle
NBT	nitro blue tetrazolium
PBS	phosphate buffered saline
PC	phosphatidylcholine
PS	phosphatidylserine
PnA	cis-parinaric (9Z,11E,13E,15Z-octadecatetraenoic) acid
RB	rose bengal
RNO	p-nitrosodimethylaniline

ROS	reactive oxygen species
TAT	protein transduction domain of Human Immunodeficiency Virus 1 trans-activating transcriptional activator
TMPD	N,N,N′,N′-tetramethyl-1,4-phenylenediamine
TMR	tetramethylrhodamine

References

1. Berg K, Selbo PK, Prasmickaite L, Tjelle TE, Sandvig K, Moan J, Gaudernack G, Fodstad O, Kjolsrud S, Anholt H, Rodal GH, Rodal SK, Hogset A. Photochemical internalization: a novel technology for delivery of macromolecules into cytosol. Cancer Res. 1999; 59:1180–1183. [PubMed: 10096543]
2. Berg K, Prasmickaite L, Selbo PK, Hellum M, Bonsted A, Hogset A. Photochemical internalization (PCI)--a novel technology for release of macromolecules from endocytic vesicles. Oftalmologia. 2003; 56:67–71. [PubMed: 12886687]
3. Endoh T, Sisido M, Ohtsuki T. Spatial regulation of specific gene expression through photoactivation of RNAi. Journal of controlled release: official journal of the Controlled Release Society. 2009; 137:241–245. [PubMed: 19376174]
4. Berg K, Selbo PK, Weyergang A, Dietze A, Prasmickaite L, Bonsted A, Engesaeter BO, Angell-Petersen E, Warloe T, Frandsen N, Hogset A. Porphyrin-related photosensitizers for cancer imaging and therapeutic applications. J Microsc. 2005; 218:133–147. [PubMed: 15857375]
5. Valenzeno DP. Photomodification of biological membranes with emphasis on singlet oxygen mechanisms. Photochem Photobiol. 1987; 46:147–160. [PubMed: 3303072]
6. Maiolo JR 3rd, Ottinger EA, Ferrer M. Specific redistribution of cell-penetrating peptides from endosomes to the cytoplasm and nucleus upon laser illumination. J Am Chem Soc. 2004; 126:15376–15377. [PubMed: 15563153]
7. Srinivasan D, Muthukrishnan N, Johnson GA, Erazo-Oliveras A, Lim J, Simanek EE, Pellois JP. Conjugation to the Cell-Penetrating Peptide TAT Potentiates the Photodynamic Effect of Carboxytetramethylrhodamine. PLoS ONE. 2011; 6:e17732. [PubMed: 21423812]
8. Matsushita M, Noguchi H, Lu YF, Tomizawa K, Michiue H, Li ST, Hirose K, Bonner-Weir S, Matsui H. Photo-acceleration of protein release from endosome in the protein transduction system. FEBS Lett. 2004; 572:221–226. [PubMed: 15304352]
9. Bourre L, Giuntini F, Eggleston IM, Mosse CA, Macrobert AJ, Wilson M. Effective photoinactivation of Gram-positive and Gram-negative bacterial strains using an HIV-1 Tat peptide-porphyrin conjugate. Photochemical & photobiological sciences: Official journal of the European Photochemistry Association and the European Society for Photobiology. 2010; 9:1613–1620. [PubMed: 20931134]
10. Wang JT, Giuntini F, Eggleston IM, Bown SG, MacRobert AJ. Photochemical internalisation of a macromolecular protein toxin using a cell penetrating peptide-photosensitiser conjugate. Journal of controlled release: official journal of the Controlled Release Society. 2012; 157:305–313. [PubMed: 21889554]
11. Sibrian-Vazquez M, Hao E, Jensen TJ, Vicente MG. Enhanced cellular uptake with a cobaltacarborane-porphyrin-HIV-1 Tat 48–60 conjugate. Bioconjugate chemistry. 2006; 17:928–934. [PubMed: 16848399]
12. Sehgal I, Sibrian-Vazquez M, Vicente MG. Photoinduced cytotoxicity and biodistribution of prostate cancer cell-targeted porphyrins. Journal of medicinal chemistry. 2008; 51:6014–6020. [PubMed: 18839477]
13. Redmond RW, Kochevar IE. Spatially resolved cellular responses to singlet oxygen. Photochem Photobiol. 2006; 82:1178–1186. [PubMed: 16740059]
14. Eggeling C, Widengren J, Rigler R, Seidel CA. Photobleaching of Fluorescent Dyes under Conditions Used for Single-Molecule Detection: Evidence of Two-Step Photolysis. Anal Chem. 1998; 70:2651–2659. [PubMed: 21644785]

15. Geissbuehler M, Spielmann T, Formey A, Marki I, Leutenegger M, Hinz B, Johnsson K, Van De Ville D, Lasser T. Triplet imaging of oxygen consumption during the contraction of a single smooth muscle cell (A7r5). Biophys J. 2010; 98:339–349. [PubMed: 20338856]
16. Muthukrishnan, N.; Johnson, G.; Erazo-Oliveras, A.; Pellois, JP. Photochem Photobiol. 2012. Synergy Between Cell-Penetrating Peptides and Singlet Oxygen Generators Leads to Efficient Photolysis of Membranes.
17. Tamm LK. Membrane insertion and lateral mobility of synthetic amphiphilic signal peptides in lipid model membranes. Biochim Biophys Acta. 1991; 1071:123–148. [PubMed: 1854792]
18. Peitzsch RM, McLaughlin S. Binding of acylated peptides and fatty acids to phospholipid vesicles: pertinence to myristoylated proteins. Biochemistry. 1993; 32:10436–10443. [PubMed: 8399188]
19. Ingersoll CM, Strollo CM. Steady state fluorescence anisotropy to investigate flavonoids binding to proteins. Journal of Chemical Education. 2007; 84:1313–1315.
20. Lakovicz, JR. Principles of Fluorescence Spectroscopy. 3. Springer; Baltimore MD: 2006.
21. Grossweiner LI, Patel AS, Grossweiner JB. Type I and Type II mechanisms in the photosensitized lysis of phosphatidylcholine liposomes by hematoporphyrin. Photochem Photobiol. 1982; 36:159–167. [PubMed: 7122710]
22. Goyal GC, Blum A, Grossweiner LI. Photosensitization of liposomal membranes by hematoporphyrin derivative. Cancer Res. 1983; 43:5826–5830. [PubMed: 6227382]
23. Kraljić I, Mohsni SE. A new method for the detection of singlet oxygen in aqueous solutions. Photochem Photobiol. 1978; 28:577–581.
24. Kochevar IE, Redmond RW. Photosensitized production of singlet oxygen. Methods Enzymol. 2000; 319:20–28. [PubMed: 10907495]
25. Tegos GP, Anbe M, Yang C, Demidova TN, Satti M, Mroz P, Janjua S, Gad F, Hamblin MR. Protease-stable polycationic photosensitizer conjugates between polyethyleneimine and chlorin(e6) for broad-spectrum antimicrobial photoinactivation. Antimicrob Agents Chemother. 2006; 50:1402–1410. [PubMed: 16569858]
26. Umezawa N, Arakane K, Ryu A, Mashiko S, Hirobe M, Nagano T. Participation of reactive oxygen species in phototoxicity induced by quinolone antibacterial agents. Arch Biochem Biophys. 1997; 342:275–281. [PubMed: 9186488]
27. Yamakoshi Y, Umezawa N, Ryu A, Arakane K, Miyata N, Goda Y, Masumizu T, Nagano T. Active oxygen species generated from photoexcited fullerene (C60) as potential medicines: O2-* versus 1O2. J Am Chem Soc. 2003; 125:12803–12809. [PubMed: 14558828]
28. Choi HS, Kim JW, Cha YN, Kim C. A quantitative nitroblue tetrazolium assay for determining intracellular superoxide anion production in phagocytic cells. J Immunoassay Immunochem. 2006; 27:31–44. [PubMed: 16450867]
29. Evans WH, Hardison WG. Phospholipid, cholesterol, polypeptide and glycoprotein composition of hepatic endosome subfractions. Biochem J. 1985; 232:33–36. [PubMed: 2867761]
30. Guha S, Rajani M, Padh H. Identification and characterization of lipids from endosomes purified by electromagnetic chromatography. Indian J Biochem Biophys. 2007; 44:443–449. [PubMed: 18320843]
31. Foote CS. Definition of Type I and Type II photosensitized oxidation. Photochemistry and Photobiology. 2008; 54:659. [PubMed: 1798741]
32. Gandin E, Lion Y, Vandevorst A. Quantum Yield of Singlet Oxygen Production by Xanthene Derivatives. Photochemistry and Photobiology. 1983; 37:271–278.
33. Mathai S, Smith TA, Ghiggino KP. Singlet oxygen quantum yields of potential porphyrin-based photosensitisers for photodynamic therapy. Photochemical & photobiological sciences: Official journal of the European Photochemistry Association and the European Society for Photobiology. 2007; 6:995–1002. [PubMed: 17721599]
34. DeRosa MC, Crutchley RJ. Photosensitized singlet oxygen and its applications. Coordination Chemistry Reviews. 2002; 233–234:351–371.
35. Natera JE, Massada WA, Amat-Guerri F, García NA. Elementary processes in the eosin-sensitized photooxidation of 3,3′-diaminobenzidine for correlative fluorescence and electron microscopy. Journal of Photochemistry and Photobiology A: Chemistry. 2011; 220:25–30.

36. Bors W, Saran M, Michel C. Pulse-radiolytic investigations of catechols and catecholamines II. Reactions of Tiron with oxygen radical species. Biochimica et Biophysica Acta (BBA) - General Subjects. 1979; 582:537–542.
37. Tavares A, Dias SRS, Carvalho CMB, Faustino MAF, Tome JPC, Neves MGPMS, Tome AC, Cavaleiro JAS, Cunha A, Gomes NCM, Alves E, Almeida A. Mechanisms of photodynamic inactivation of a Gram-negative recombinant bioluminescent bacterium by cationic porphyrins. Photochemical & Photobiological Sciences. 2011; 10
38. Aizenman E. Modulation of N-methyl-d-aspartate receptors by hydroxyl radicals in rat cortical neurons in vitro. Neuroscience Letters. 1995; 189:57–59. [PubMed: 7603627]
39. Girotti AW. Lipid hydroperoxide generation, turnover, and effector action in biological systems. J Lipid Res. 1998; 39:1529–1542. [PubMed: 9717713]
40. Smith LL, Hill FL. Detection of sterol hydroperoxides on thin-layer chromatoplates by means of the Wurster dyes. J Chromatogr. 1972; 66:101–109. [PubMed: 5019185]
41. Williams SL, Kirkpatrick I, Worrall DR. Electron transfer reactions in ternary systems on silica gel surfaces: evidence for radical cation diffusion. Photochemical & photobiological sciences: Official journal of the European Photochemistry Association and the European Society for Photobiology. 2010; 9:937–941. [PubMed: 20464021]
42. Kriska T, Girotti AW. Separation and quantitation of peroxidized phospholipids using high-performance thin-layer chromatography with tetramethyl-p-phenylenediamine detection. Anal Biochem. 2004; 327:97–106. [PubMed: 15033516]
43. Girotti AW. Translocation as a means of disseminating lipid hydroperoxide-induced oxidative damage and effector action. Free Radical Biology & Medicine. 2008; 44:956–968. [PubMed: 18206663]
44. Kobayashi T, Stang E, Fang KS, de Moerloose P, Parton RG, Gruenberg J. A lipid associated with the antiphospholipid syndrome regulates endosome structure and function. Nature. 1998; 392:193–197. [PubMed: 9515966]
45. Chen B, Jiang Y, Zeng S, Yan J, Li X, Zhang Y, Zou W, Wang X. Endocytic sorting and recycling require membrane phosphatidylserine asymmetry maintained by TAT-1/CHAT-1. PLoS Genet. 2010; 6:e1001235. [PubMed: 21170358]
46. Volinsky R, Cwiklik L, Jurkiewicz P, Hof M, Jungwirth P, Kinnunen PK. Oxidized phosphatidylcholines facilitate phospholipid flip-flop in liposomes. Biophys J. 2011; 101:1376–1384. [PubMed: 21943418]

HIGHLIGHTS

- TAT peptide labeled with fluorophore binds to negatively charged phospholipids
- Binding to lipids brings fluorophore in close proximity to membrane bilayer
- Excitation of Fl-CPP causes ROS production and photo-oxidation of membrane lipids
- Membrane photodamage by Fl-CPPs requires presence of arginines within CPP sequence
- Fluorophore and CPP act synergistically to destroy membranes upon irradiation

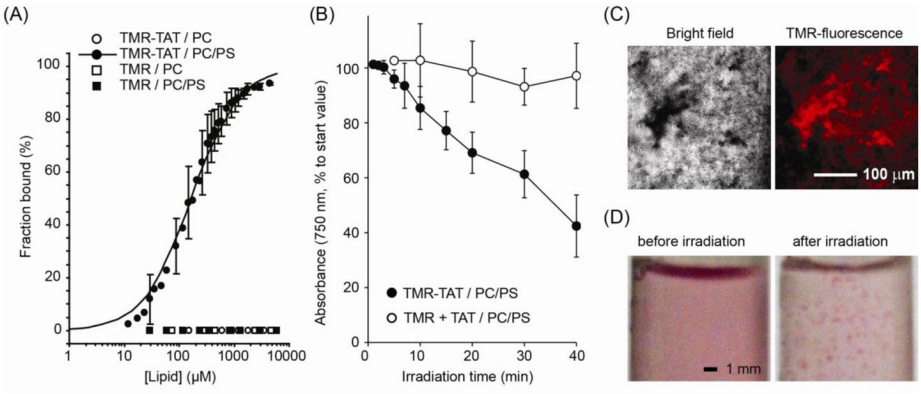

Figure 1.

TMR-TAT binds to negatively charged LUVs and induces photodamage to these LUVs selectively.

A) Fraction of TMR and TMR-TAT bound to PC or PC/PS LUVs as a function of total lipid concentration. Binding was evaluated by titrations of fluorescence anisotropy of samples and their conversion to fraction bound taking in account change of fluorescence quantum yield of bound fluorophores. The solid line represented for the binding of TMR-TAT with PC/PS LUVs corresponds to the best fit obtained from a one site-specific binding model (R-value= 0.95). B) Irradiation of PC/PS LUVs with TMR-TAT (2 μM; peptide to total lipids ratio P:L is 1:400) causes loss of turbidity of liposomal dispersion. This is not observed when PC/PS LUVs, TMR (2 μM) and unlabeled TAT (2 μM) are irradiated, or with other control conditions (including incubation in dark or after illumination of neutral PC LUVs with TMR-TAT, data not shown). All experiments were performed in triplicates (averages and corresponding standard deviations are represented). C) Irradiation of PC/PS LUVs with TMR-TAT is accompanied by formation of fluorescent liposomal aggregates, observed by bright field and fluorescence microscopy. D) At high doses of irradiation, large aggregates are directly visible to human eye (photographs of liposome suspensions in test tubes are shown, the pink color being is due to TMR-TAT).

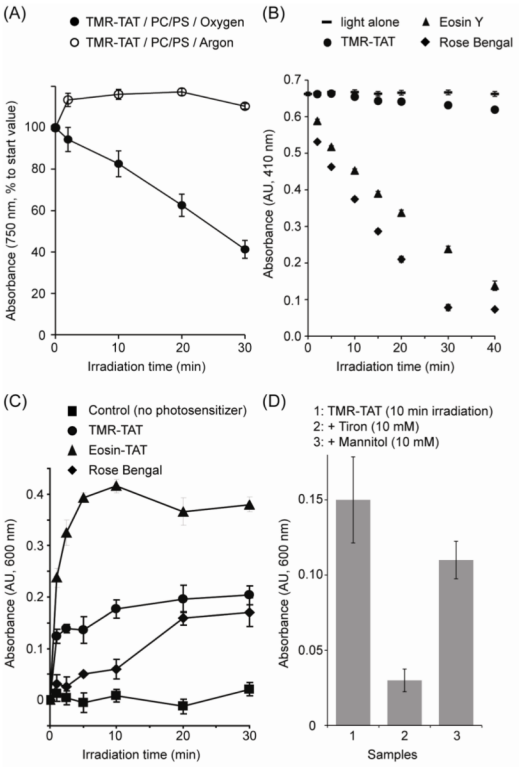

Figure 2.

TMR-TAT-induced photodamage is osygen dependent and TMR-TAT produces singlet oxygen and superoxide.

A) Dependence of photolytic efficiency of TMR-TAT (as evaluated by turbidometry) on oxygen. The graph shows difference in relative turbidity change for PC/PS LUVs irradiated with TMR-TAT (2 μM, P:L=1:400) in samples alternatively saturated with argon or oxygen gas prior to experiment. B) Detection of singlet oxygen photo-generation by the RNO assay, performed with TMR-TAT and eosin-TAT and Rose Bengal as positive controls (all at 7 μM). C) Detection of superoxide phot-generation by the NBT assay, performed with TMR-TAT, eosin-TAT and Rose Bengal (all at 10 μM). D) Effect of the quenchers tiron and mannitol on the chemical reduction of NBT mediated by irradiation of TMR-TAT. Samples were treated with TMR-TAT as described in C) with the exception that tiron (10 mM) or mannitol (10 mM) were added prior to irradiation. All experiments were performed in triplicates (averages and corresponding standard deviations are represented).

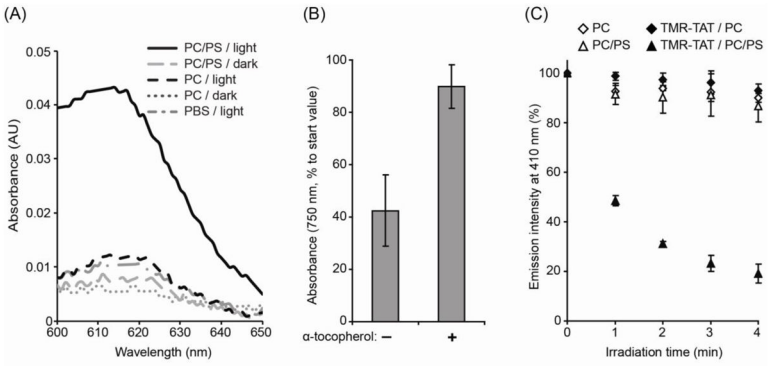

Figure 3.

Irradiation of TMR-TAT mediates the oxidative damage of lipids in PC/PS LUVs.

A) Irradiation of PC/PS LUVs with TMR-TAT results in the formation of lipid peroxides visualized by reaction with TMPD and the production of “Wurster’s Blue” coloration of oxidized cation-radical with a characteristic absorption near 610 nm. B) The lipophilic anti-α-tocopherol inhibits the photodestruction of PC/PS LUVs after 40 min of irradiation with TMR-TAT (2 μM, P:L=1:400). C) Evaluation of relative oxidation conditions created in lipid membrane by using the oxidation reporter PnA. PnA (1% total lipids) was added to PC and PC/PS LUVs and its oxidation is monitored by measuring the loss of fluorescence that accompanies the irradiation of LUVs without and with TMR-TAT (2 μM, P:L=1:400). All experiments were performed in triplicates (averages and corresponding standard deviations are represented).

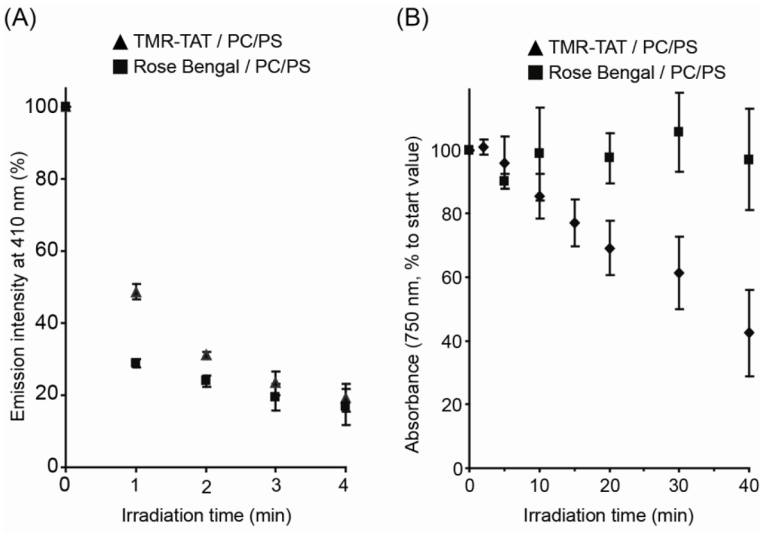

Figure 4.

TMR-TAT causes the photo-oxidation and photodestruction of PC/PS LUVs while the photosensitizer RB only mediates photo-oxidation.

A) RB (2 μM) and TMR-TAT (2 μM, P:L=1:400) cause a similar decrease in PnA fluorescence upon irradiation of PC/PS LUVs. (b) Irradiation of RB and PC/PS LUVs is not accompanied by a loss of turbidity as seen with TMR-TAT. All experiments were performed in triplicates (averages and corresponding standard deviations are represented).

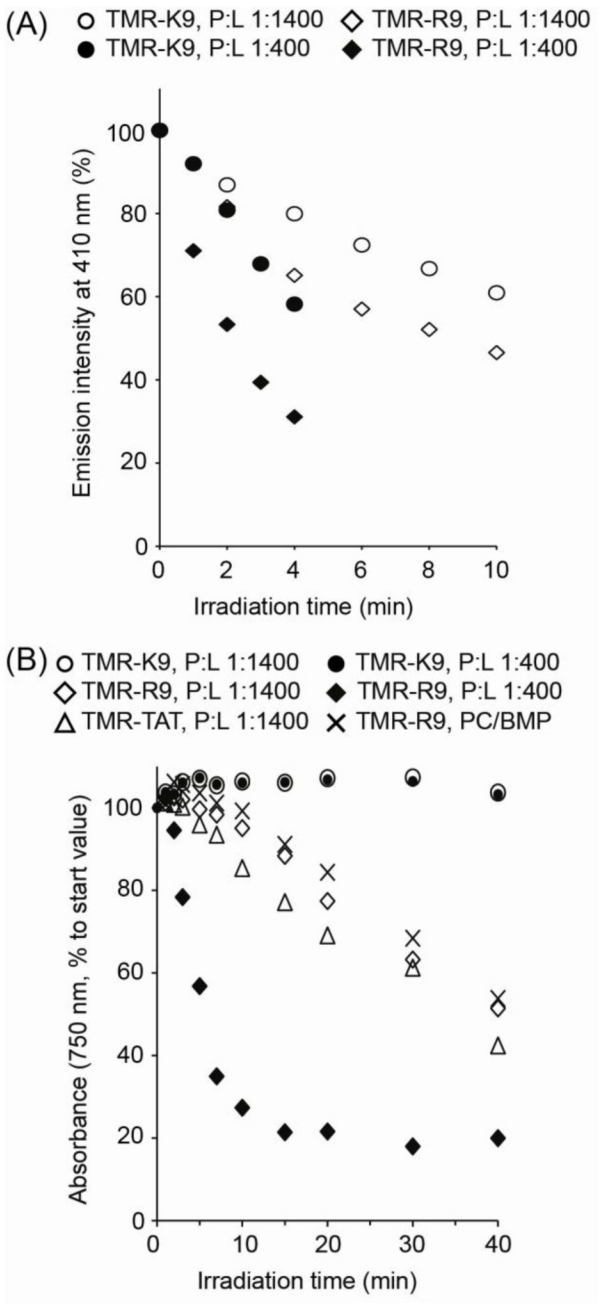

Figure 5.

TMR-R9 and TMR-K9 both promote the oxidation of PC/PS LUVs but only irradiation of TMR-R9 leads to liposomal photo-destruction.

A) Oxidation of PnA in PC/PS LUVs irradiated with TMR-R9 and TMR-K9 at P:L ratios of 1:1400 and 1:400. B) Loss of turbidity and photodestruction of PC/PS LUVs illuminated with TMR-K9, TMR-TAT and TMR-R9 at P:L ratios of 1:1400 and 1:400 (effect of TMR-TAT on PC/PS LUVs at P:L=1:400 is similar to that of TMR-R9, data not shown). The photodescruction of PC/BMP liposomes by TMR-R9 at a P:L of 1:400 is also presented. All experiments were performed in triplicates. The data presented corresponds to the average values calculated. The standard deviations are 10% or less of the value of each data point (not represented for clarity).